Ultrasound in Med. & Biol., Vol. 46, No. 5, pp. 1142–1157, 2020

0301-5629/$ - see front matter

https://doi.org/10.1016/j.ultrasmedbio.2020.01.022

● *Original Contribution*

QUANTITATIVE ULTRASOUND MONITORING OF BREAST TUMOUR RESPONSE TO NEOADJUVANT CHEMOTHERAPY: COMPARISON OF RESULTS AMONG CLINICAL SCANNERS

Lakshmanan Sannachi,*,† Mehrdad Gangeh,*,† Ali-Sadeghi Naini,*,†,‡ Priya Bhargava,† Aparna Jain,† William Tyler Tran,†,‡ and Gregory Jan Czarnota*,†,‡

* Department of Medical Biophysics, University of Toronto, Toronto, ON, Canada; † Physical Sciences, Sunnybrook Research Institute, Sunnybrook Health Sciences Centre, Toronto, ON, Canada; and ‡ Department of Radiation Oncology, Sunnybrook Health Sciences Centre, Toronto, Canada

(*Received* 24 *September* 2018; *revised* 17 *January* 2020; *in final from* 20 *January* 2020)

Abstract—Quantitative ultrasound (QUS) techniques have been demonstrated to detect cell death *in vitro* and *in vivo*. Recently, multi-feature classification models have been incorporated into QUS texture-feature analysis methods to increase further the sensitivity and specificity of detecting treatment response in locally advanced breast cancer patients. To effectively incorporate these analytic methods into clinical applications, QUS and texture-feature estimations should be independent of data acquisition systems. The study here investigated the consistencies of QUS and texture-feature estimation techniques relative to several factors. These included the ultrasound system properties, the effects of tissue heterogeneity and the effects of these factors on the monitoring of response to neoadjuvant chemotherapy. Specifically, tumour-response–detection performance based on QUS and texture parameters using two clinical ultrasound systems was compared. Observed variations in data between the systems were small and the results exhibited good agreement in tumour response predictions obtained from both ultrasound systems. The results obtained in this study suggest that tissue heterogeneity was a dominant feature in the parameters measured with the two different ultrasound systems; whereas differences in ultrasound system beam properties only exhibited a minor impact on texture features. The McNemar statistical test performed on tumour response prediction results from the two systems did not reveal significant differences. Overall, the results in this study demonstrate the potential to achieve reliable and consistent QUS and texture-based analyses across different ultrasound imaging platforms. (E-mail: Gregory.Czarnota@sunnybrook.ca)

Key Words: **Breast cancer, Neoadjuvant chemotherapy, Quantitative ultrasound, Texture analysis, Therapy response monitoring.**

INTRODUCTION

Ultrasound scattering from biologic tissue contributes to diagnostic information in medical ultrasound. In conventional gray-scale imaging, tissue characteristics are interpreted from variations in image brightness, normally obtained from the envelope of ultrasound radiofrequency (RF) signals. However, such images only use a fraction of the information available in RF signals. In contrast, quantitative ultrasound (QUS) methods provide more detailed information about tissue properties, based on fundamental acoustic attributes of tissue (Insana and Hall 1990).

Address correspondence to: Dr. Gregory J. Czarnota, Department of Radiation Oncology, Sunnybrook Health Sciences Centre, 2075, Bayview Avenue, Toronto, ON M4 N 3 M5, Canada. E-mail: Gregory.Czarnota@sunnybrook.ca

QUS techniques have been used in various tissue characterization applications such as the differentiation between normal and fatty liver (Ghoshal et al. 2012), the diagnosis of ocular tumours, the characterization of prostate cancer (Feleppa et al. 1997) and breast masses (Tadayyon et al. 2014) and the studies of cardiac and vascular abnormalities (Yang et al. 2007). In these applications, the QUS parameters such as mid-band fit (MBF), spectral slope (SS), 0-MHz spectral intercept (SI), integrated backscatter coefficient, average scatterer diameter (ASD) and average acoustic concentration (AAC) were measured using QUS analysis methods (Insana and Hall 1990; Feleppa et al. 1997; Lizzi et al. 1997). In several preclinical studies, such parameters have been used for detecting tumour response to various treatments such as chemotherapy, photodynamic therapy, radiation therapy

and ultrasound-mediated microbubble therapy (Banihashemi et al. 2008; Vlad et al. 2008, 2009; Czarnota et al. 2012; Lee et al. 2012). Newer texture-based analyses of QUS parametric maps have shown a strong correlation to biologic changes in tissue, such as apoptosis, a programmed form of cell death (Sadeghi-Naini et al. 2013a, 2014). Recently, QUS techniques have been used in locally advanced breast cancer (LABC) treatment response monitoring studies. LABC is an aggressive form of breast cancer that comprises a wide range of clinical presentations including T3/T4 disease, tumour with size greater than 5 cm or extensive axillary lymph node involvement. Very recently, multi-feature classification models have been developed based on QUS and texture features to detect the response of LABC to neoadjuvant chemotherapy early after the start of treatment, with accuracies above 80% (Sadeghi-Naini et al. 2017).

For tumour response detection to be translated into a clinical application, QUS and QUS-texture features must be reproducible across different equipment platforms and transducers. Studies have evaluated tissue mimicking phantoms with known properties to demonstrate agreement between different ultrasound equipment platforms (Anderson et al. 2010; Nam et al. 2011; Nam et al. 2012a, 2012b). Scattering properties of animal tumours have also been examined using 3 clinical ultrasound systems and 1 laboratory ultrasound system with a total of 9 different transducers. Results there demonstrated reasonable agreements between the backscatter coefficient measurements acquired on the different systems (Wirtzfeld et al. 2010).

Recently, QUS parameters obtained from treated mouse tumours, using a single-element, high-frequency transducer and a conventional low-frequency linear array transducer were compared (Sadeghi-Naini et al. 2013b). The results demonstrated an increase in the MBF and SI parameter values after treatment, using both low- and high-frequency ultrasound. The magnitude of the change in QUS parameters after treatment differed as expected between low- and high-frequency ultrasound. For example, increases in MBF after 24 h of treatment were +6 dB, and +3.5 dB for conventional low- and high-frequency ultrasound, respectively. The differences in magnitudes may have been attributable to the following variations in transducer characteristics: axial and lateral resolution and frequency bandwidth, which can affect the measurement of tissue scattering properties. To date, a comparison of QUS measurements in a clinical breast cancer model, using multiple ultrasound imaging platforms, has not been performed.

In this study, first, the consistencies of QUS and texture-feature estimation techniques were investigated in terms of their dependence on several factors, including ultrasound system characteristics and tissue heterogeneity. Second, the effects of these factors on the monitoring of responses to neoadjuvant chemotherapy were also investigated. Finally, the performance of two computer-assisted tumour response monitoring systems based on multi-feature classification models, proposed in Sadeghi-Naini et al. (2017), were evaluated using clinical data sets acquired using two different ultrasound systems. In general, the results obtained in this study suggest that it is possible to obtain agreement among QUS parameters and QUS-based texture measurements from different clinical ultrasound systems. The work demonstrates the potential to conduct tumour response monitoring using QUS and QUS-based texture parameters.

MATERIALS AND METHODS

Patients and clinical data

A total of 24 LABC patients were enrolled in a tumour response monitoring study approved by the Sunnybrook Research Institute (Toronto, ON, Canada) research ethics board. All 24 patients signed an informed consent form before participating in this study. Standard therapy for LABC consisted of a multimodality treatment. Treatment in these patients started with neoadjuvant chemotherapy to facilitate tumour shrinkage and metastatic control. This was followed by surgery and then radiation therapy. Chemotherapy was chosen based on the histologic type of breast cancer, its grade and disease stage and the patient's overall health status. Chemotherapy was administered as a combination of several drugs to achieve a more effective response. All LABC patients underwent breast surgery after the completion of neoadjuvant chemotherapy, based on institutional guidelines. The choice for surgery (mastectomy or breast conserving surgery [BCS]) was at the discretion of the surgeon and the patient based on the response of the tumour to neoadjuvant chemotherapy and the feasibility of preserving the breast (Cho et al. 2013; Barranger et al. 2015; Sun et al. 2017). After surgery (mastectomy/BCS), radiation therapy was used to increase the locoregional control rate and overall survival (Hortobagyi 1990; Senkus et al. 2015; National Comprehensive Cancer Network 2016; Rubovszky and Horváth 2017). Before treatment, as part of their clinical care, all patients were subjected to a core needle biopsy to confirm a cancer diagnosis, and to obtain information regarding histologic subtype and hormone receptors status such as estrogen receptor (ER), progesterone receptor (PR) and human epidermal growth factor receptor 2 (HER2). Mastectomy specimens were examined by a board-certified pathologist, using whole-mount 5" × 7" pathology slides digitized using a confocal scanner (TISSUEscope, Huron Technologies, Waterloo, ON, Canada). The standard approach to determine tumour

pathologic response to chemotherapy was based on surgical histopathology. Systematic techniques such as the Miller and Payne score were used to describe pathologic response to chemotherapy based on the cellular and histopathologic characteristics of the tumour (Ogston et al. 2003). In this study, patients were divided into 2 groups based on Miller-Payne scores from their pathology reports. Patients with a Miller-Payne score of 3−5 and more than a 30% reduction in tumour size compared with pre-treatment size were classified as responders (R). Patients with a Miller-Payne score of 1 or 2 and less than 30% reduction in tumour size were defined as non-responders (NR).

Ultrasound systems and scanning protocol

Ultrasound RF data were acquired from breast tumours using two clinical systems: an Ultrasonix−RP ([ULX] Ultrasonix Medical Corp., Richmond, BC, Canada), and a GE−LOGIQ E9 ([GE] Healthcare, Milwaukee, WI, USA). The ULX was used with an L14-5/60 transducer, operating at a center frequency of 6.3 MHz. After scanning with the ULX device, the GE—equipped with a 9 L-D linear array transducer, operating at a center frequency of 6 MHz—was also used to scan the breast. Physical and beam properties for the ULX's L14-5/60 and GE's 9 L-D linear array transducers are summarized in Table 1. Transducer beam properties, including axial resolution, lateral resolution and depth of focus, were measured using a wire-target technique with a wire diameter of 180 μm (Raum and O'Brien1997). Ultrasound data were acquired from breast tumour volumes before treatment; then at weeks 1, 4 and 8 after the start of treatment; and before surgery, with both the ULX and GE clinical systems. Depending on tumour size, 4−6 image planes were acquired at 1-cm intervals across the breast tumour volume, with the transducer focus at the mid-depth of the tumour. Scan focal depths remained consistent for individual patients throughout the study. All breast tumours were scanned by placing a linear array transducer in the radial direction with respect to the tumour.

Table 1. Physical parameters and beam parameters of L14-5/60 (ULX) and 9 L-D (GE) linear array transducers

Parameters	Ultrasonix − RP L14-5/60	GE-LOGIQ 9 L-D
Number of elements	128	192
Kerf width [μm]	25	23
Element width [μm]	477	207
Elevation [mm]	4	6
Elevation focus [mm]	14	28
Depth of focus (−6 dB) [mm]	16.7	28.1
Centre frequency [MHz]	6.3	6.0
Frequency bandwidth range [MHz]	3−8	3.5−8.5
f-number	1.82	3.33
Axial resolution at 15 mm (−6 dB) [μm]	198	420
Lateral resolution at 15 mm (−6 dB) [μm]	483	1231

Ultrasound data analysis

For each scan, 4−6 image planes were acquired. The tumour region of interest (ROI) was selected by a radiologist for all tumour RF data frames. Each ROI was divided into window blocks ($15\lambda \times 15\lambda$), using a Hanning window with a specific overlap percentage along the axial and lateral directions as discussed later in this report. Here, λ is the wavelength at the center frequency. The power spectral density was computed by taking the square magnitude of the fast Fourier transform of the gated RF signal. In this study, each window block was assumed to contain uniform diffuse scatterers (Yao et al. 1990). Based on this assumption, the power spectra computed from the gated RF signals within each window block were averaged for further processing. In several tissue characterization studies (Lizzi et al. 1983; Oelze and Zachary 2006; Vlad et al. 2009), a data reduction method, using a plane reflector, was utilized for accurate backscatter property estimation from the ultrasound data acquired with unfocused or focused single element disk transducers. However, for more complex transducers, such as arrays, a reference phantom method was subsequently proposed to remove system dependent effects in backscatter property estimation (Yao et al. 1990). In this current study, the sample spectrum was normalized using a reference phantom to account for instrumental and transmission path factors. In the reference phantom method, the sample power spectrum is normalized by dividing the measured power spectrum by the spectrum from a reference phantom. The intervening tissue and tumour attenuations were compensated before determining tumour scatter parameters from the normalized power spectrum. A breast attenuation coefficient of 1 dB/MHz/cm was assumed for the intervening tissue, including skin, subcutaneous fat and fibroglandular tissue, based on published attenuation coefficients (Duric et al. 2005). The tumour attenuation was estimated using a reference phantom method (Labyed and Bigelow 2011). For tumour attenuation estimation, the backscatter coefficient was assumed to be constant within the selected ROI (parameter estimation region). To obtain the attenuation, the linear rate of decrease in the log-transformed normalized power spectrum, with the depth in the ROI at each frequency, was calculated. The attenuation coefficient divided by frequency, for the frequency bandwidth of 3−8 MHz, was then averaged. The reference phantom used in this study consisted of glass beads (5−30 μm) embedded in a homogeneous background of microscopic oil droplets in gelatin. This reference

phantom was prepared at the Medical Physics Department, University of Wisconsin, Madison WI, USA, and sent to the Department of Electrical and Computer Engineering, University of Illinois, Urbana, IL, USA, for the measurement of ultrasonic properties. The attenuation coefficient and speed of sound were measured in through-transmission, using the insertion loss and the arrival time difference techniques (Kremkau et al. 1981; Madsen et al. 1982), respectively. A total of 4 spherically focused transducers with center frequencies of 2.5, 5, 7.5 and 10 MHz were used for this measurement. The attenuation coefficient and speed of sound of the reference phantom were 0.786 dB/MHz/cm and 1540 m/s, respectively. The backscatter coefficient of the reference phantom was measured using the method proposed by Insana and Hall (Insana et al. 1990; Insana and Hall 1990), in which the power spectra of reflected RF waveforms were compared with the spectrum of a plane reflector at the same axial position, after compensation for attenuation of an intermediate medium. Four spherically focused transducers with centre frequencies of 1.5, 3.5, 7.5 and 13 MHz were used to calculate backscatter coefficients for the frequency range 1.5−20 MHz.

The tumour spectral parameters—MBF, SS and SI—were determined from the log-compressed, attenuation-compensated, normalized power spectrum by linear regression analysis over the frequency bandwidth. The ASD and AAC were derived from the backscatter coefficient, ($\sigma_m(f)$) obtained from the normalized spectrum as follows:

$$\sigma_m(f,Z) = \frac{\overline{S_m(f,Z)}}{\overline{S_r(f,Z)}}\sigma_r(f)e^{4(\alpha_m(f)Z_m+\alpha_i(f)Z_i-\alpha_i(f)Z)} \quad (1)$$

where $S_m(f, Z)$ and $S_r(f, Z)$ are power spectra of the tumour and reference phantom, respectively; $\sigma_m(f, Z)$ and $\sigma_r(f)$ are backscatter coefficients of the tumour and reference phantom, respectively; $Z\ (= Z_m + Z_i)$ is depth of the window block ($15\lambda \times 15\lambda$) with respect to the transducer; f is frequency in MHz. Z_i and Z_m are the depth of the intervening tissue/tumour interface with respect to the transducer and depth of the window block with respect to the intervening tissue/tumour interface, respectively; and $\alpha_m(f)$, $\alpha_i(f)$ and $\alpha_r(f)$ are the attenuation coefficients of the tumour, intervening tissue and reference phantom, respectively. Then ASD and AAC were estimated by comparing the theoretically derived backscatter coefficient ($\sigma_{theor}(f)$), using a spherical Gaussian scatterer form factor model (Oelze and O'Brien 2002; Gerig et al. 2003), to the measured backscatter coefficient using a least-squares method.

$$FF_{Gaussian}(f, a_{eff}) = exp(-0.827(k.a_{eff})) \quad (2)$$

$$\sigma_{theor}(f) = Cf^4 a_{eff}^6 \overline{n}\gamma_0^2 FF_{Gaussian}(f, a_{eff}) \quad (3)$$

where $FF_{Gaussian}(f, a_{eff})$ is the Gaussian form factor; a_{eff} is the scatter size and k is the wave number. The constant $C$is equal to $\pi^4/36c^4$ and c is the speed of sound in the medium. In this study, a speed of sound of 1540 m/s was assumed for breast tissue. This value is consistent with ultrasound tomography−derived measurement of speed of sound in the breast (Li et al. 2009). The product of the average number of scatters per unit volume, $\overline{n}$, and the mean-square variation in acoustic impedance between a scatterer and the surrounding medium, γ_0^2, is the scattering strength or acoustic concentration.

The scatterer spacing (SAS), which is the spacing between two adjacent scatterers was determined using an autoregressive spectral analysis method by modeling the tumour echo signal as an autoregressive signal (Wear et al. 1993). The order of the autoregressive model was selected based on general features from tissue histopathology images. The ultrasound frequency used in this study can detect microstructures approximately 250 μm in size. This is comparable to lobule diameters observed from histopathology images. The spacing between the lobules was in the range of 200−900 μm. The order of the autoregressive model, the p value, was selected based on this spacing distance. A p value of 50 was set to the maximum value of the SAS detectable by this method. Finally, color-coded parametric maps were developed for each estimated QUS parameter by generating a spatial map of the parameter values computed over all window blocks. Equivalent pixel resolution QUS parametric maps were obtained from the ULX and GE ultrasound system RF signals by adjusting the overlap percentage based on their axial and lateral resolutions. For the ULX system data, a window overlap percentage of 95% (axial) × 99% (lateral) was used. For the GE system data, a window overlap of 94% (axial) × 91% (lateral) was used.

In addition to the mean values of QUS parameters, which were determined by averaging QUS parametric map pixel values, spatial distributions of QUS parameters in parametric maps were evaluated using a gray-level co-occurrence matrix (GLCM) (Haralick et al. 1973) method, which represents the angular relationship between neighboring pixels as well as their distances in parametric maps. A total of 16 symmetric GLCMs were constructed for each parametric map, considering each pixel's neighbors are located at different distances and directions (*i.e.*, at distances of 1, 2, 3 and 4 pixels and at angles of 0°, 45°, 90° and 135°). From each symmetric GLCM, 4 texture features—specifically, the contrast (CON), correlation (COR), homogeneity (HOM) and energy (ENE)—were determined and averaged. Hence, in this study, a total of 24 textural features (4 texture

features from each of MBF, SS, SI, ASD, AAC and SAS parametric maps) were computed. A total of 31 features (6 mean of QUS parameters, 24 texture features and ACE) were determined from tumour data. All QUS and texture parameters were estimated from tumour RF data acquired at weeks 1, 4 and 8 after treatment, using the ULX and GE ultrasound systems.

Classification of patient response to treatment

To characterize tumour response to treatment, multi-parametric classification models proposed in our earlier study were used (Sadeghi-Naini et al. 2017). Those classification models were developed based on a 100 LABC patient QUS and texture-feature data set (81 responders and 19 non-responders) acquired with the ULX system, using a *k*-nearest neighbor classifier. The accuracies of those classification models in differentiating responders from non-responders at weeks 1, 4 and 8 after treatment initiation were reported to be 82%, 86% and 85%, respectively. Those models were applied to the QUS and texture-based parameters estimated from the 24 LABC patient ULX and GE data acquired in the present study, and tumour responses were classified separately for the 2 ultrasound system data sets.

Consistency analysis

Before performing tumour response detection, the consistencies of QUS and texture-feature estimation techniques were investigated with respect to several factors. These factors included measurement stability, ultrasound system characteristics and tissue heterogeneity. First, the measurement stability, which represented variations in QUS parameter estimation over time and between users, was determined for the ULX and GE clinical systems by acquiring RF signals from a homogeneous phantom for 10 times at 1-h intervals during a period of 10 h by several users. The phantom was made of glass beads 82.5 ± 7.5 μm in diameter, immersed in agar (attenuation and speed of sound were 0.715 dB/MHz/cm and 1540 m/s, respectively). The root mean square deviations over time and user ($RMSD_{t,\ user}$) in the estimated parameters were calculated using

$$RMSD_{t,user} = \sqrt{\frac{\sum_{t=1}^{N}\left(\hat{Q} - Q_{t,user}\right)^2}{N}}, \quad (4)$$

where, $Q_{t,user}$ is the estimated parameter acquired at time t by a particular user, N is the number of scans and $\hat{Q}$ is the average of N estimated parameters. The Faran model (Faran 1951) was used to extract ASD and AAC values from the backscatter coefficient of the homogeneous phantom.

To investigate the effect of tissue heterogeneity on the mean QUS and texture-based parameters, the parameters were calculated from 5−6 acquired frames from 5 breast tumours and compared with a homogeneous phantom, using the ULX and GE systems. Those 5 tumours were selected from the responder group with a molecular type of ER+/PR+/Her2− and size range from 5.8−10.4 cm. The root mean square differences between parameters extracted from scanned frames ($RMSD_f$) were subsequently calculated as follows:

$$\mathrm{RMSD_f} = \sqrt{\frac{\sum_{f=1}^{N}\left(\hat{Q} - Q_f\right)^2}{N}}, \quad (5)$$

where, $\hat{Q}$ is the averaged QUS parameter, Q_f is the QUS parameter from each individual frame and N is the number of frames.

To investigate the effect of clinical ultrasound system properties on parameter estimation, the root mean square differences between averaged QUS data sets ($RMSD_{USS}$) acquired using the ULX and GE clinical systems for the phantoms and breast tumours were calculated using

$$\mathrm{RMSD_{USS}} = \sqrt{\frac{\sum_{n=1}^{N}\left(\hat{Q}(ULX)_n - \hat{Q}(GE)_n\right)^2}{N}}, \quad (6)$$

where, $\hat{Q}(ULX)$ and $\hat{Q}(GE)$ are the averaged QUS or texture parameters estimated from the ULX and GE ultrasound data, respectively. Here, averaged means were computed over frames, and N is the number of samples (N = 1 for phantom and N = 5 for tumour). In this study, a total of 31 features were determined from RF data. However, for a consistency analysis of QUS and texture-parameter estimation in this study, a few features were specifically selected, including MBF, SS and MBF texture parameters. The MBF parameter has been demonstrated to be one of the most sensitive parameters to detect cell death induced by cancer therapy in breast tumours (Sadeghi-Naini et al. 2013b, 2013c, 2014, 2017). Therefore, the variation of mean and texture features extracted from MBF parametric maps were for the most part examined in this consistency analysis.

Statistical analysis

Statistical tests were conducted to compare the parameters determined from responders and non-responders at weeks 1, 4 and 8, and to compare the responder and non-responder groups determined from ULX and GE data separately. To determine which type of statistical test to use for comparing the response groups, a Shapiro-Wilk normality test was performed on each parameter to assess whether it demonstrated a normal distribution. For group comparisons, an unpaired *t*-test was used for the data that passed the normality

test; otherwise, a Mann-Whitney unpaired test was used. To compare the ULX and GE data, pairwise comparisons were performed on each response group, using a paired *t*-test for normally distributed data and a Wilcoxon paired test for non-normally distributed data. The Bland-Altman method (Bland and Altman 1986) was used to evaluate the agreement between the ULX and GE systems. In this method, the limits of agreement were defined by the average difference ± 1.96 standard deviations of the difference. Here, 'difference' refers to the difference between parameter values estimated from ULX and GE data. An F-test (Shen and Faraway 2004) was used to compare the power spectrum and backscatter coefficient curves calculated from the ULX and GE data. The McNemar test (McNemar 1947) was used to compare the tumour responses determined from ULX and GE data sets. Statistical significance was considered for results with a $p < 0.05$.

RESULTS

Consistency analysis of QUS and texture parameter measurements

In the consistency analysis studies, the variations in QUS and texture parameters over time and between users ($RMSD_{t,user}$) were calculated first. For example, deviations in QUS parameters, MBF, SS, SI, ASD and AAC estimated from ULX data were 0.084 dB, 0.0178 dB/MHz, 0.123 dB, 0.457 μm and 0.491 dB/cm^3, respectively; whereas the same QUS parameters estimated from GE data were 0.065 dB, 0.016 dB/MHz, 0.046 dB, 0.128 μm and 0.299 dB/cm^3. The $RMSD_{t,user}$ in the MBF-based texture parameters, MBF-CON, MBF-COR, MBF-ENE and MBF-HOM calculated from ULX data were 0.228, 0.025, 0.004 and 0.007, respectively. Those calculated from GE data were 0.210, 0.021, 0.003 and 0.006, respectively.

Representative B-mode images, normalized power spectra and backscatter coefficients as a function of frequency acquired from a homogeneous phantom and an untreated heterogeneous breast tumour, using the ULX (L14-5/60) and GE (9 L-D) systems, are presented in Figure 1. The phantom power spectra and backscatter coefficient results indicated only small variations between multiple frames acquired with each ultrasound system. Average curves from both systems intersected and demonstrated good agreement in magnitude. The F-test was used to compare averaged power spectra and backscatter coefficient curves obtained with the ULX and GE systems. F-tests conducted on the averaged log-transformed power spectra and backscatter coefficients from the homogeneous phantom did not indicate significant differences ($p = 0.29$ and $p = 0.72$, respectively) over the analysis bandwidth. Similarly, representative averaged power spectra and backscatter coefficient curves acquired from a breast tumour, using the ULX and GE systems, intersected. However, the variations of power spectra and backscatter coefficient between frames were comparably higher than the difference between averaged curves. Whereas the F-test conducted on the averaged power spectra determined from a representative breast tumour did not indicate significant differences ($p = 0.08$) between the 2 systems, there was a significant difference ($p = 0.04$) detected in the backscatter coefficients between the 2 systems.

Representative MBF parametric maps overlaid on B-mode images acquired from a homogeneous phantom and a representative heterogeneous breast tumour with the ULX and GE clinical systems are presented in Figure 2. Tables 2 and 3 present QUS and texture parameters estimated from the phantom and a representative tumour, using the GE and ULX clinical ultrasound systems. Analyses indicated that there was close agreement between the results generated by these 2 systems. Compared with results from the phantom, the $RMSD_f$ calculated for the representative tumour indicated larger variations in QUS and texture-based parameters estimated. For example, the variation in the MBF parameter observed between scanned frames acquired from the phantom and a representative tumour were 0.12 dB and 1.22 dB, respectively. To investigate further, root mean square differences ($RMSD_{USS}$) between averaged parameters were calculated and tests for statistical significance of differences were performed between multiple-frame parameters for these 2 systems. As expected, the differences between the estimated tumour parameters measured using the GE and ULX systems were larger than those corresponding to phantom-based measurements. Moreover, the variations between the frames ($RMSD_f$) measured in tumour QUS and texture-based parameters were comparably higher than the variations between averaged ULX and GE parameters ($RMSD_{USS}$). Statistical tests, however, did not reveal significant differences between the parameters estimated using data from the ULX and GE devices. The range of *p*-values obtained from the tests of statistically significant differences between all QUS parameters acquired from 2 ultrasound systems, and between all texture parameters acquired from two ultrasound systems were 0.406−0.566 and 0.133−0.289, respectively. Finally, an ROI consistency analysis study was conducted on data from 5 patients. In this study, ROIs sizes were reduced to 80% and increased to 110% of the original size. The relative changes in the MBF values for 80% and 110% changes of the original ROIs sizes were 6.4% and 2.7%, respectively.

Results of the consistency analysis studies on QUS and texture-based parameters are summarized in Figure 3. These indicate that the variation in QUS

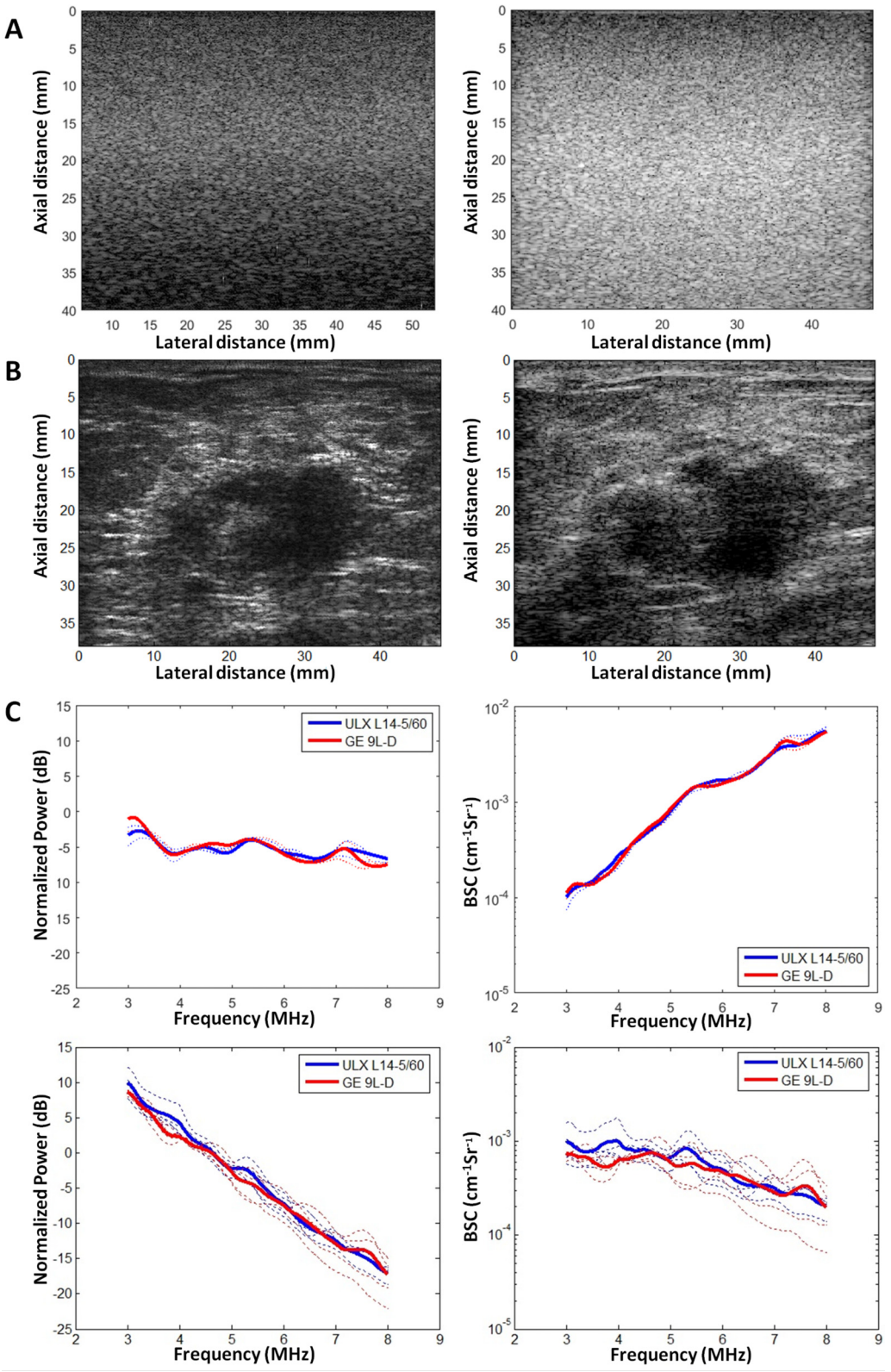

Fig. 1. (a) Phantom B-mode images from the ULX (*left*) and GE (*right*) systems. (b) B-mode images from a representative heterogeneous breast tumour from the ULX (*left*) and GE (*right*) systems. (c) Normalized power spectra (*left*), backscatter coefficients (*right*) from a homogeneous phantom (*top*) and a representative heterogeneous breast tumour (*bottom*) from ULX and GE data. Data from acquired frames (*dotted lines*) are presented as well as data averaged over all frames (*solid lines*).

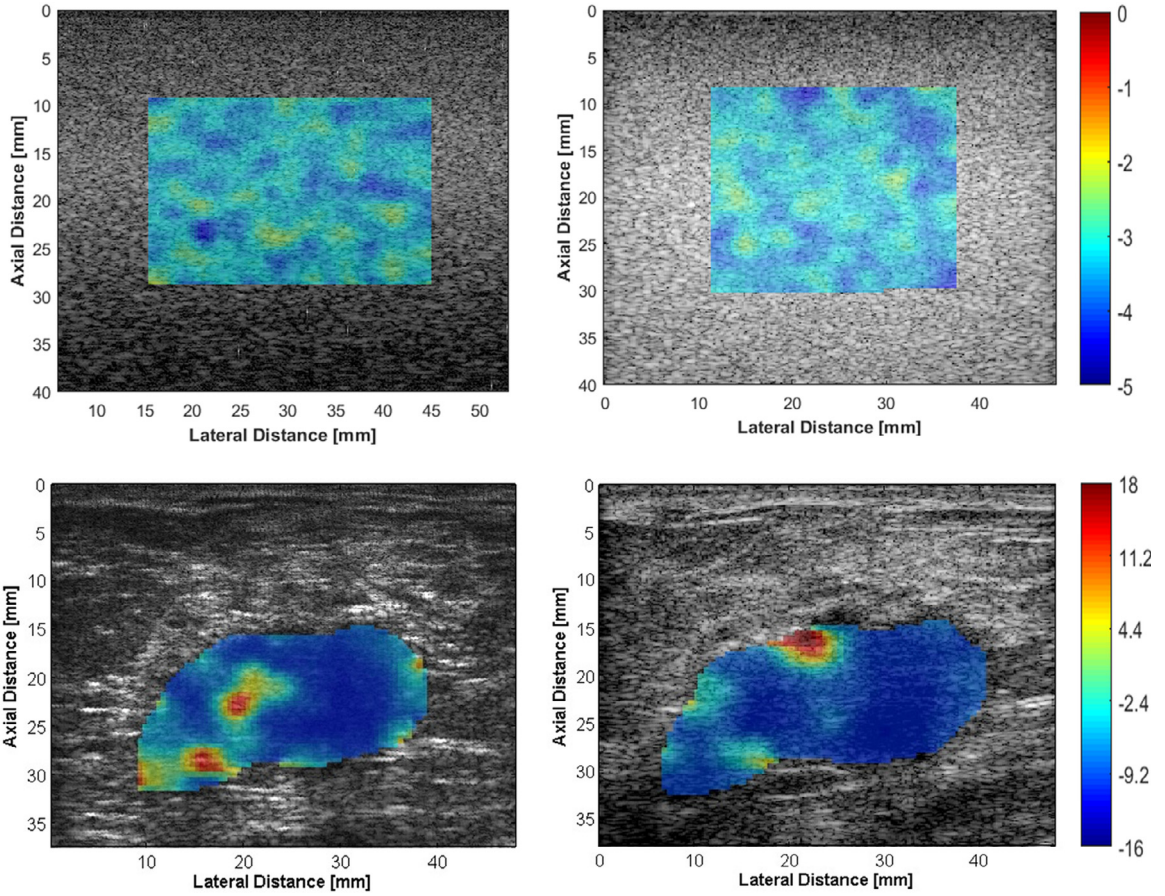

Fig. 2. Representative MBF (dB) parametric images of a homogeneous phantom (*top*) and a breast tumour (*bottom*) from ULX (*left*) and GE (*right*) data. Here, dB is with respect to the value of backscatter power spectrum of the reference phantom at the centre frequency.

parameters is for the most part attributable to the tissue heterogeneity and that the variation in texture-based parameters is owing to both tissue heterogeneity and ultrasound system properties.

Comparison of estimated parameters in LABC response monitoring

Having established the level of consistency of each ultrasound system with respect to the other, data for tumour response assessment was collected from 24 patients receiving chemotherapy, and results from the two systems were compared. Patient characteristics, tumour properties and treatments administered are summarized in Appendix Table A.1. The patients were between 36 and 73 y of age with a mean age of 53 y. Tumour sizes ranged from 2.1–10.9 cm, with a mean of 5.7 cm. A total of 92% of patients had invasive ductal carcinoma and the remaining 8% had either invasive

Table 2. $RMSD_f$ of QUS parameters attributable to tissue heterogeneity calculated from both ultrasonic systems and $RMSD_{USS}$ between mean QUS parameters acquired with those systems

RMSD	Phantom				Tumour			
	MBF *[dB]*	SS *[dB/MHz]*	SI *[dB]*	AAC [dB/cm^3]	MBF *[dB]*	SS *[dB/MHz]*	SI *[dB]*	AAC [dB/cm^3]
QUS(ULX)	-2.86 ± 0.11	0.03 ± 0.01	-3.03 ± 0.11	122.86 ± 0.57	-5.52 ± 0.81	-2.92 ± 0.21	21.59 ± 1.53	108.76 ± 0.86
QUS(GE)	-2.91 ± 0.06	-0.09 ± 0.03	-2.36 ± 0.13	122.07 ± 0.63	-5.05 ± 1.11	-2.77 ± 0.29	20.32 ± 1.56	108.23 ± 0.94
$RMSD(ULX)_f$	0.14	0.03	0.19	0.38	0.96	0.23	1.64	0.97
$RMSD(GE)_f$	0.10	0.07	0.61	0.53	1.22	0.35	1.65	1.30
$RMSD_{USS}$	0.14	0.07	0.72	0.32	0.47	0.14	1.27	0.53
p value*	0.268	0.157	0.346	0.623	0.617	0.579	0.379	0.257

* Associated with the statistical comparison of multiple-frame QUS-parameters with these systems.

Table 3. $RMSD_f$ of MBF-textures attributable to tissue heterogeneity calculated from both ultrasonic systems data as well as the $RMSD_{USS}$ between MBF-based parameters acquired with those systems

RMSD	Phantom				Tumour			
	MBF-CON	MBF-COR	MBF-ENE	MBF-HOM	MBF-CON	MBF-COR	MBF-ENE	MBF-HOM
Texture (ULX)	4.305 ± 1.247	0.580 ± 0.048	0.029 ± 0.006	0.550 ± 0.027	4.338 ± 0.744	0.722 ±0.041	0.025 ± 0.004	0.574 ± 0.021
Texture (GE)	3.798 ± 1.159	0.566 ± 0.024	0.037 ± 0.010	0.563 ± 0.033	4.881 ± 0.807	0.716 ± 0.031	0.021 ± 0.003	0.537 ± 0.019
$RMSD\ (ULX)_f$	0.086	0.014	0.004	0.012	0.706	0.038	0.008	0.020
$RMSD\ (GE)_f$,	0.160	0.023	0.003	0.007	0.737	0.028	0.006	0.018
$RMSD_{USS}$	0.372	0.032	0.008	0.012	0.543	0.005	0.005	0.037
p value*	0.143	0.078	0.402	0.945	0.193	0.485	0.087	0.063

* From statistical tests comparing multiple-frame MBF-based texture parameters using these systems.

lobular carcinoma or invasive micropapillary carcinoma. Ultrasound data were collected from patients before treatment, and at weeks 1, 4 and 8 during treatment with the ULX and GE systems. QUS methods were applied to data acquired from both systems and MBF, SS, SI, ASD, AAC and SAS parametric images were constructed. Representative QUS parametric images constructed for a responder using both systems over the course of treatment are presented in Figure 4. The average changes in QUS parameters estimated for responders and non-responders using both ultrasound systems over the course of treatment are presented in Figure 5a. The QUS parameters estimated from both systems indicated similar trends over all treatment times. Significant differences in QUS parameters between the two populations of responders and non-responders, as determined from clinical response metrics, are indicated by an asterisk in Figure 5a. Specifically, MBF and AAC values calculated from ULX and GE data exhibited significant differences between clinically responding and non-responding patients after treatment. Statistical testing of significance was also performed on changes in QUS parameters acquired with the ULX and GE systems for the responder and non-responder groups, separately. None of the QUS parameters indicated a significant difference between the ULX and GE data. This was true for both responder, and non-responder groups. The $RMSD_{USS}$ calculated for breast tumour MBF, SS, SI, ASD and AAC parameters

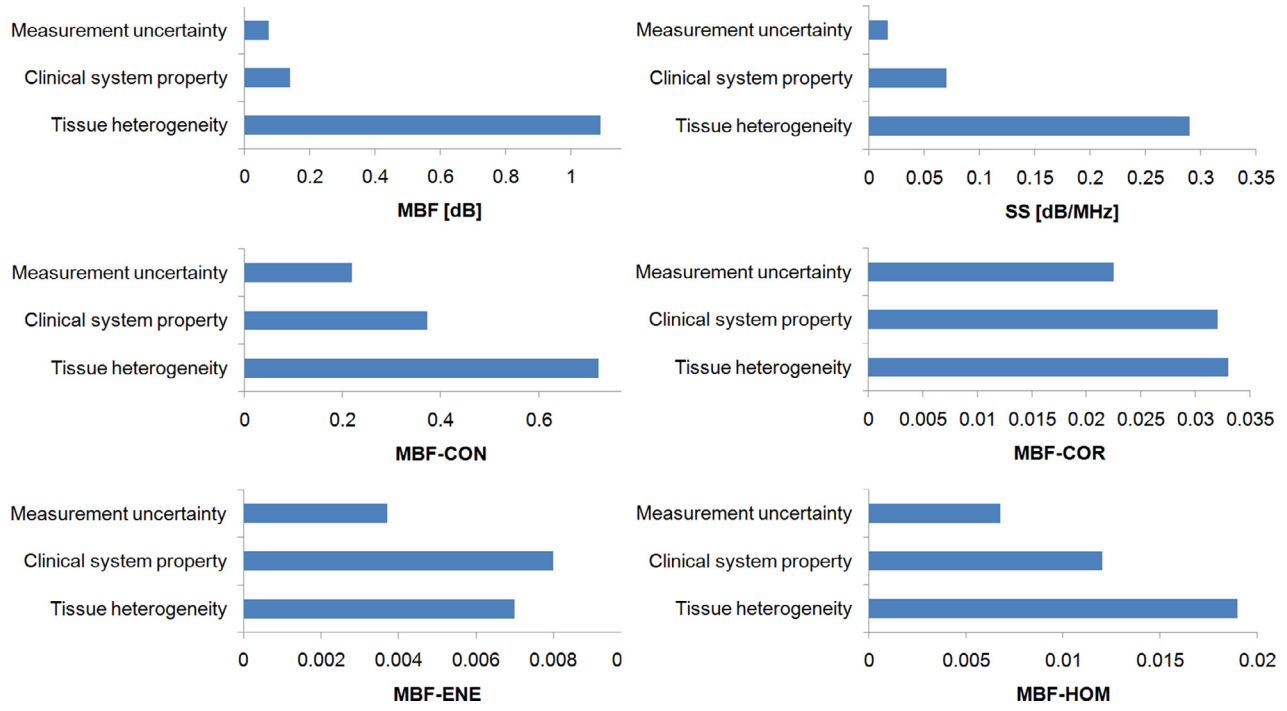

Fig. 3. The root mean square deviation or differences in QUS parameters, MBF and SS, and MBF-texture parameters, MBF-CON, MBF-COR, MBF-ENE and MBF-HOM attributable to measurement uncertainty, variations in clinical system beam properties and tissue heterogeneity.

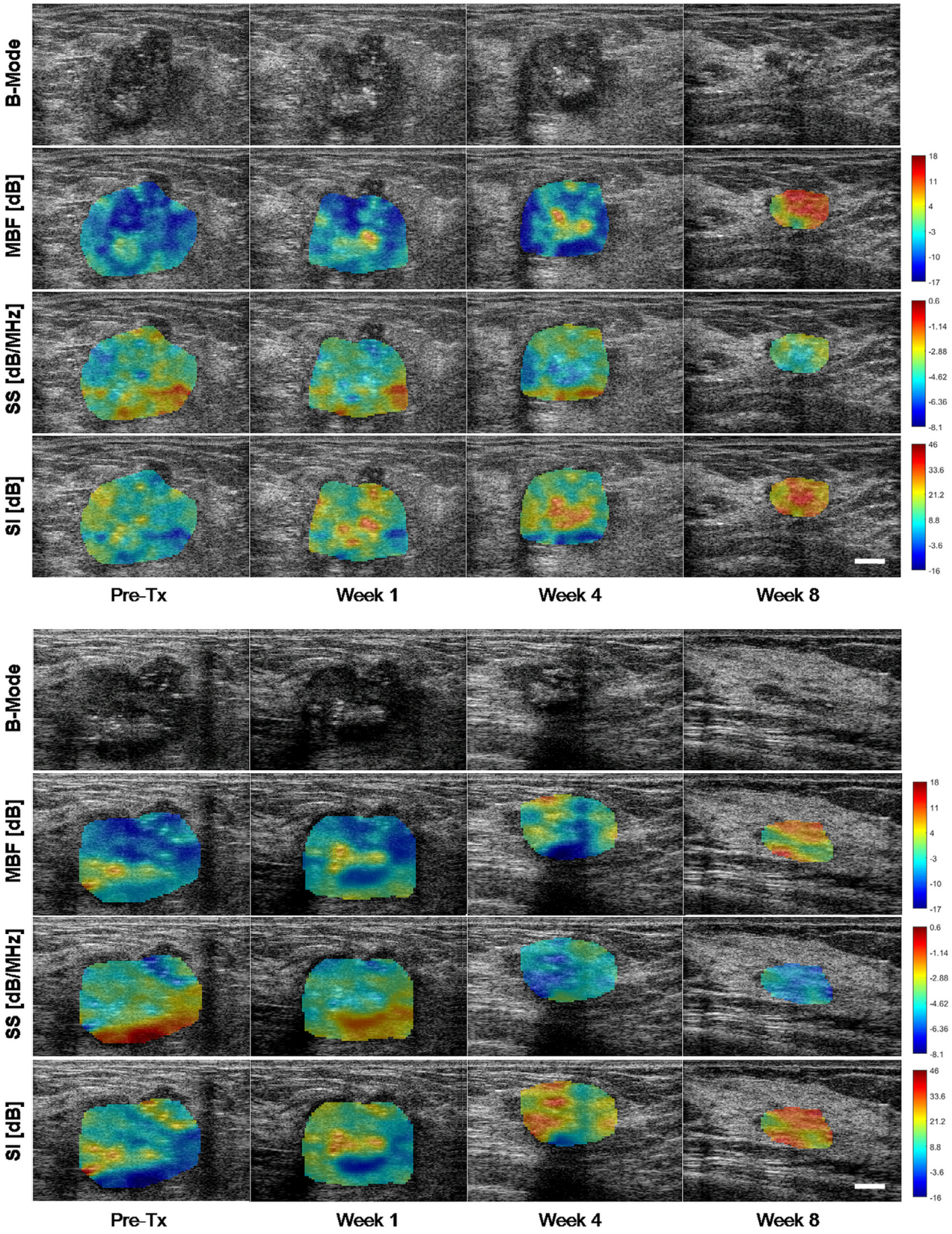

Fig. 4. B-mode MBF, SS and SI parametric images from a responder before treatment (Pre-Tx) as well as at weeks 1, 4 and 8 during treatment acquired using the ULX (*top*) and GE (*bottom*) systems. The *white scale bars* in ultrasound images represent 5 mm.

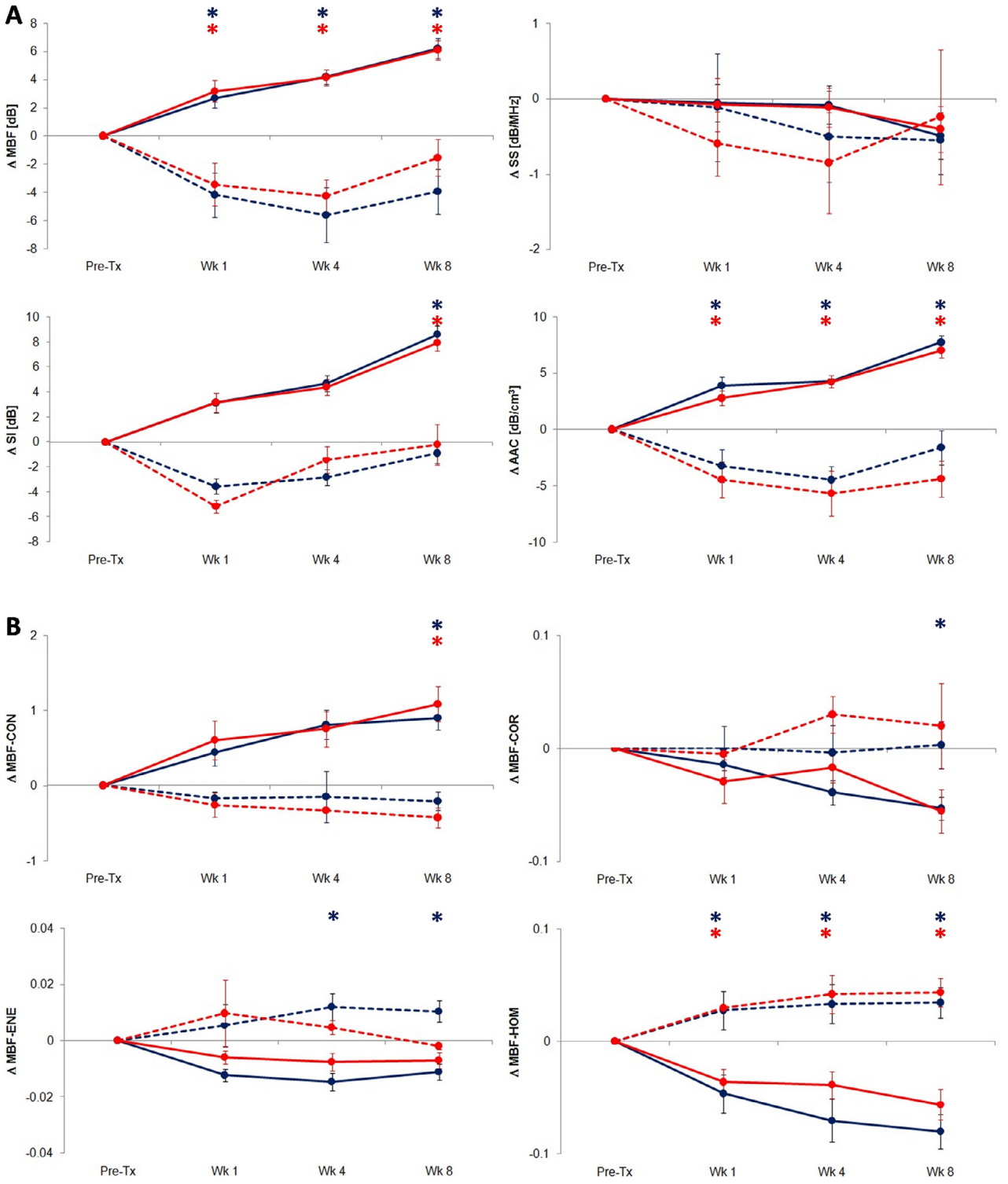

Fig. 5. (a) The mean changes in QUS parameters, MBF, SS, SI and AAC and (b) the MBF-based texture parameters, MBF-CON, MBF-COR, MBF-ENE and MBF-HOM measured in clinical responders (*solid line*) and non-responders (*dotted line*) throughout the course of treatment for the ULX (*blue line*) and GE (*red line*) systems. The asterisk (*) represents a significant difference ($p < 0.05$) based on the ANOVA test.

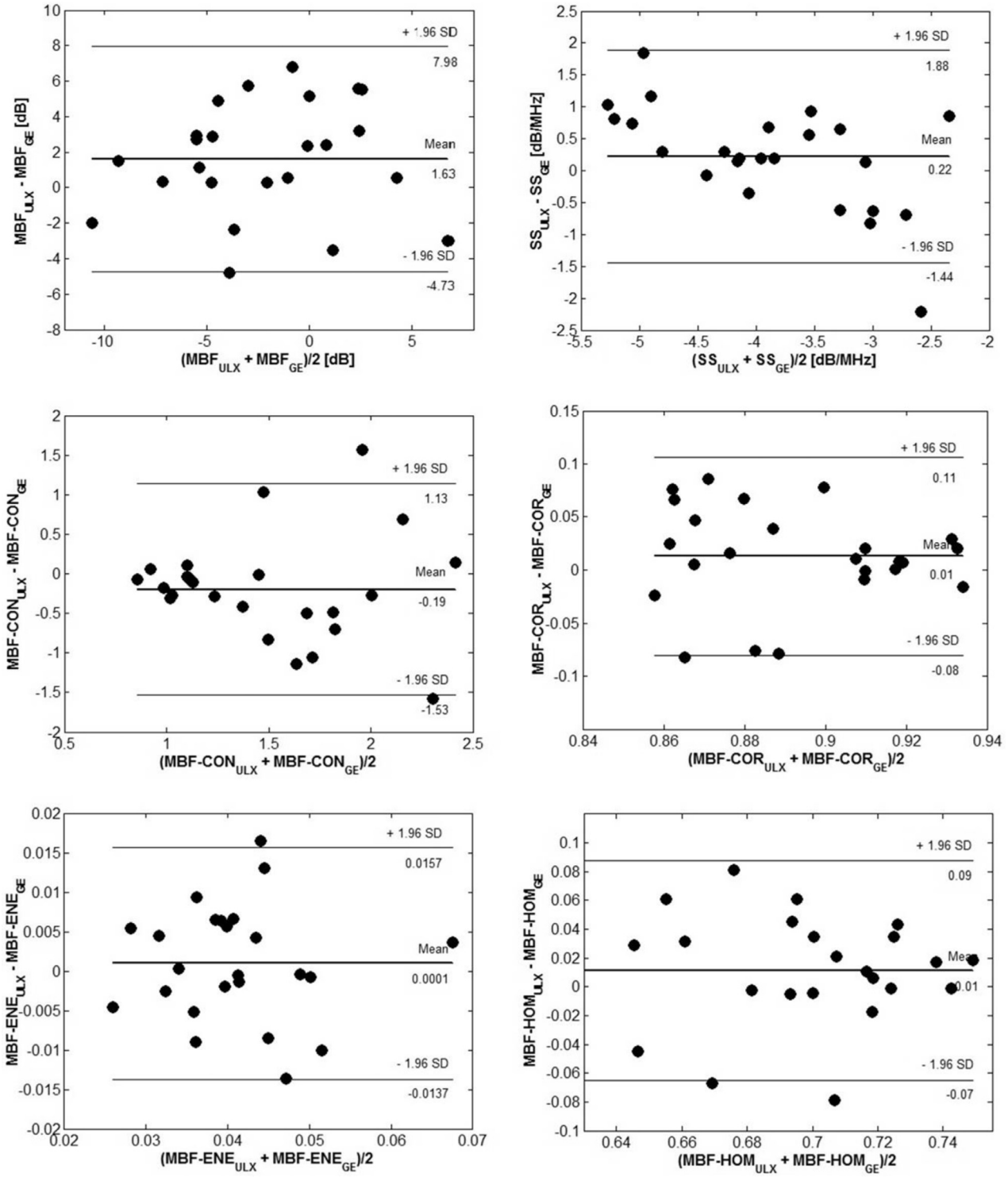

Fig. 6. Bland–Altman plots comparing QUS and QUS-based texture parameters acquired from breast tumours, using the ULX and GE ultrasound systems. The limits of agreement between the 2 clinical system parameters are defined by the mean difference ± 1.96 standard deviation of differences.

acquired before treatment exhibited small differences at 1.71 dB, 0.22 dB/MHz, 4.21 dB, 2.04 μm and 1.29 dB/cm^3, respectively.

Average changes in MBF-texture parameters estimated for responders and non-responders using the data obtained from the ULX and GE systems over the course

Table 4. The classification results of chemotherapy response at weeks 1, 4 and 8 after the beginning of treatment using the ULX and GE parameters based on the proposed models

Scan time	US system	Sensitivity [%]	Specificity [%]	Accuracy [%]	McNemar p*
Week 1	ULX	60.0	50.0	58.8	0.752
	GE	60.0	50.0	58.8	
Week 4	ULX	78.9	66.7	77.3	0.545
	GE	64.3	66.7	69.1	
Week 8	ULX	71.4	100.0	73.3	0.683
	GE	71.4	100.0	73.3	

* Results between treatment response predictions from the two ultrasound systems.

of treatment are presented in Figure 5b. The magnitudes of texture parameters extracted from both data sets were comparable. Most texture parameters demonstrated similar trends occurring with treatment time. None of the texture parameters indicated differences between the ULX and GE data for either the responder or the non-responder groups. The $RMSD_{USS}$ calculated for breast tumour MBF-CON, MBF-COR, MBF-ENE and MBF-HOM features before treatment exhibited small differences with values of 0.82, 0.06, 0.02 and 0.08, respectively.

Bland-Altman plots were used to evaluate the agreement between the ULX and GE systems when used for breast tumour response monitoring. Bland-Altman plots for QUS parameters, MBF and SS and MBF-based texture parameters, MBF-CON, MBF-COR, MBF-ENE and MBF-HOM acquired from breast tumours before treatment with the two clinical systems are presented in Figure 6. The limits of agreement between parameters from the 2 clinical systems were defined by the mean difference $\pm$ 1.96 standard deviations of the difference. Figure 6 indicates that approximately 92% of breast cancer patients' parameters determined from the GE data were comparable with those estimated from the ULX data.

Each patient's response to treatment was predicted by submitting their ULX and GE parameters acquired at weeks 1, 4 and 8 to a response classification algorithm proposed in our earlier study (Sadeghi-Naini et al. 2017). The treatment response detection results are summarized in Table 4. The treatment response predictions determined using ULX and GE data sets were compared by performing a McNemar test. The p-values obtained from the McNemar test (0.75, 0.55 and 0.68 at weeks 1, 4 and 8, respectively) revealed no significant differences between the classification results obtained from the 2 clinical systems.

DISCUSSION

In this study QUS and QUS-based texture parameters acquired from breast cancer patients receiving neoadjuvant chemotherapy were compared, using an Ultrasonix-RP and a GE-LOGIQ E9 clinical ultrasound system. As a first step, the influence of various factors, including ultrasound system and tissue properties, were analyzed to determine their effects on the estimation of QUS and texture parameters.

The frequency bandwidths of the two clinical ultrasound systems were comparable. There were some differences in the QUS parameters determined, most likely attributable to variations in beam properties. Specifically, comparing the statistical test p-values of the parameters estimated from the ULX and GE systems revealed that differences in ultrasound system beam properties, such as axial and lateral resolution, had a greater effect on the texture-based features than mean QUS parameters. However, those differences were very small, and results exhibited good agreement between the two ultrasound systems when tested on phantom data. F-tests conducted on averaged power spectra and backscatter coefficients, using a homogeneous phantom, did not exhibit significant differences between the ULX and GE data. Compared with variations observed in estimated parameters resulting from all system and tissue dependent effects, the variation caused by tissue heterogeneity was higher.

To determine the sensitivity of the parameters to tissue heterogeneity, we investigated both mean QUS and texture-based parameters, using data acquired from a homogeneous phantom and heterogeneous tumours. The level of agreement between the ULX and GE systems varied between the phantom and breast tumours. Variations in the parameter values between frames were higher in breast tumours than in phantom samples. Tissue heterogeneity may account for both mean QUS and corresponding texture-based parameter variations between scanners attributable to an expected limitation in acquiring identical frames. For this reason, the $RMSD_{USS}$ values calculated from breast tumours were higher than those observed in the phantom. It was observed that $RMSD_{USS}$ was higher for texture-based parameters than for mean QUS parameters.

Although the variation in mean QUS is for the most part attributable to tissue heterogeneity, the higher discrepancy in texture parameters, which represents the spatial distribution of the QUS parameters in selected tumour ROIs in 2-D space, is likely attributable to both

tissue heterogeneity and expected differences in transducer characteristics. Especially, for small tumours, there are fewer pixels in the parametric maps from which to extract texture features. Therefore, minor variations within the pixel levels related to transducer performance potentially result in larger differences between texture features acquired using the 2 ultrasound systems with different beam properties. This was reflected in texture-based parameter Bland−Altman plots. The patients close or over the limits of the agreement line (mean difference ± 1.96 standard deviation) in the Bland−Altman plots, particularly in the texture-based parameters plots (Fig. 6) are those with small tumours, such as patients 12, 22, 23 and 24 (Appendix Table A.1, with tumour sizes indicating largest tumour dimension). The ultrasound and texture parameter estimation methods used in this study suggest that the tumour ROI size selected in the ultrasound image should be a minimum of 10 mm in both axial and lateral directions. This permits an accurate estimation of tumour attenuation values and the extraction of texture features from the tumour QUS images by comparing QUS values at different pixel distances and directions, using the GLCM method. Other limitations of this study were that breast tumour speed of sound and intervening tissue attenuation values were fixed based on literature values. Backscatter parameters from tumour ultrasound RF data were also estimated based on the assumption that each window block within the tumour ROIs contains uniform diffuse scatterers. However, biologic tissues contain complex structures that may invalidate the assumption of the diffuse scatter model necessary for QUS techniques. Several studies have investigated this issue and proposed methods to reduce the effects of non-diffuse echoes in tissue backscattered signals (Luchies et al. 2012; Rosado-Mendez et al. 2016). These limitations need to be further investigated to improve accurate estimates of breast tumour backscatter properties. Nevertheless, the overall results obtained in this study indicated good agreement between the parameters estimated from breast tumours, using data from the ULX and GE clinical systems. The study identified that 92% of breast cancer patients' parameters estimated from GE data were comparable with those estimated from the ULX data.

Earlier LABC response monitoring studies (Sadeghi-Naini et al. 2013c; Sannachi et al. 2015) have reported that MBF and AAC, which are related to scatterer number density and scatterer mechanical properties (Feleppa et al. 1986), are the most effective QUS parameters for use in detecting breast tumour responses to chemotherapy. This was also demonstrated during the tumour response monitoring, using both ULX- and GE-based data presented here. The changes in mean QUS and texture-based parameters acquired with the ULX and GE clinical systems exhibited similar trends throughout the course of treatment. However, there were expected minor differences in the magnitude of estimated parameters attributable to various ultrasonic system and tissue properties. Despite the small differences, the tumour response predicted using data from the 2 systems had good agreement. The McNemar test did not indicate significant differences between the classification results obtained from the 2 clinical systems within the performance of the prediction model used. The range of accuracy in detecting tumour response of 24 LABC patients using the model proposed in our earlier study (Sadeghi-Naini et al. 2017) was 59%−73% (Table 4). This smaller value in accuracy may be attributable to a limited number of patients in the non-responder group enrolled in this present study.

CONCLUSION

This study identified that QUS results acquired from phantom data and patients with breast tumours using 2 different ultrasound systems were comparable. The work also indicated that tissue heterogeneity, combined with data acquisition variability in 2-D scans, which limits the ability to acquire RF data from the exact same frames, was a dominant feature in causing variations in parameter values obtained from 2 different ultrasound systems. It must be noted that the number of frames used to calculate the QUS and texture-based parameters in breast tumours is very small. Acquiring a larger number of frames and 3-D analysis of tumour ultrasound data may reduce the effect of tissue heterogeneity. In the future, our work will investigate the performance of the LABC treatment response prediction by acquiring data from whole tumour, using a 3-D automated breast ultrasound system to overcome the effect of tumour heterogeneity in QUS parameter estimation. However, there is consistency in data obtained from the 2 different ultrasound systems in terms of the use of this limited frame data for therapy response monitoring. The results found in this study suggest that it is possible to obtain agreement among QUS and texture-based parameter measurements from different clinical ultrasound systems even when system properties vary. This type of agreement demonstrates the potential to base clinically relevant measurements on QUS and texture-based parameters. Nevertheless, investigations on larger cohorts of patients from more than 2 different clinical systems will be useful to evaluate the effect of system properties on QUS and texture analysis techniques very accurately in clinical settings.

Acknowledgments—This project was funded by the Terry Fox Foundation with funds from the Hecht Foundation, the Natural Sciences and Engineering Research Council of Canada and the Canadian Institutes of Health Research. Clinical trial number: ClinicalTrials. gov NCT00437879. G.J.C. was supported through a University of Toronto James and Mary Davie Chair in Breast Cancer Imaging and Ablations. The authors would like to

thank Karina Quiaoit, Elyse Watkins and Harini Suraweera for their help with collecting and organizing the clinical data.

Conflict of interest disclosure—The authors declare that they have no conflict of interest to disclose.

SUPPLEMENTARY MATERIALS

Supplementary material associated with this article can be found in the online version at doi:10.1016/j.ultrasmedbio.2020.01.022.

REFERENCES

Anderson JJ, Herd MT, King MR, Haak A, Hafez ZT, Song J, Oelze ML, Madsen EL, Zagzebski JA, O'Brien WD, Hall TJ. Interlaboratory comparison of backscatter coefficient estimates for tissue-mimicking phantoms. Ultrason Imaging 2010;32:48–64.

Banihashemi B, Vlad R, Debeljevic B, Giles A, Kolios MC, Czarnota GJ. Ultrasound imaging of apoptosis in tumor response: Novel preclinical monitoring of photodynamic therapy effects. Cancer Res 2008;68:8590–8596.

Barranger E, Antomarchi J, Chamorey E, Cavrot C, Flipo B, Follana P, Peyrottes I, Chapellier C, Ferrero JM, Ihrai T. Effect of neoadjuvant chemotherapy on the surgical treatment of patients with locally advanced breast cancer requiring initial mastectomy. Clin Breast Cancer 2015;15:231–235.

Bland JM, Altman DG. Statistical methods for assessing agreement between two methods of clinical measurement. Lancet 1986;327:307–310.

Cho JH, Park JM, Park HS, Park S, Kim S, Il, Park BW. Oncologic safety of breast-conserving surgery compared to mastectomy in patients receiving neoadjuvant chemotherapy for locally advanced breast cancer. J Surg Oncol 2013;108:531–536.

Czarnota GJ, Karshafian R, Burns PN, Wong S, Al Mahrouki A, Lee JW, Caissie A, Tran W, Kim C, Furukawa M, Wong E, Giles A. Tumor radiation response enhancement by acoustical stimulation of the vasculature. Proc Natl Acad Sci U S A 2012;109:E2033–E2041.

Duric N, Littrup P, Babkin A, Chambers D, Azevedo S, Kalinin A, Pevzner R, Tokarev M, Holsapple E, Rama O, Duncan R. Development of ultrasound tomography for breast imaging: Technical assessment. Med Phys 2005;32:1375–1386.

Faran JJ. Sound scattering by solid cylinders and spheres. J Acoust Soc Am 1951;23:405.

Feleppa EJ, Liu T, Kalisz A, Shao MC, Fleshner N, Reuter V, Fair WR. Ultrasonic spectral-parameter imaging of the prostate. Int J Imaging Syst Technol 1997;8:11–25.

Feleppa EJ, Lizzi FL, Coleman DJ, Yaremko MM. Diagnostic spectrum analysis in ophthalmology: A physical perspective. Ultrasound Med Biol 1986;12:623–631.

Gerig A, Zagzebski J, Varghese T. Statistics of ultrasonic scatterer size estimation with a reference phantom. J Acoust Soc Am 2003;113:3430–3437.

Ghoshal G, Lavarello RJ, Kemmerer JP, Miller RJ, Oelze ML. *Ex vivo* study of quantitative ultrasound parameters in fatty rabbit livers. Ultrasound Med Biol 2012;38:2238–2248.

Haralick RM, Shanmugam K, Dinstein I. Textural features for image classification. IEEE Trans Syst Man Cybern IEEE 1973;3:610–621.

Hortobagyi GN. Comprehensive management of locally advanced breast cancer. Cancer 1990;66:1387–1391.

Insana MF, Hall TJ. Parametric ultrasound imaging from backscatter coefficient measurements: Image formation and interpretation. Ultrason Imaging 1990;12:245–267.

Insana MF, Wagner RF, Brown DG, Hall TJ. Describing small-scale structure in random media using pulse-echo ultrasound. J Acoust Soc Am 1990;87:179–192.

Kremkau FW, Barnes RW, McGraw CP. Ultrasonic attenuation and propagation speed in normal human brain. J Acoust Soc Am 1981;70:29.

Labyed Y, Bigelow TA. A theoretical comparison of attenuation measurement techniques from backscattered ultrasound echoes. J Acoust Soc Am 2011;129:2316–2324.

Lee J, Karshafian R, Papanicolau N, Giles A, Kolios MC, Czarnota GJ. Quantitative ultrasound for the monitoring of novel microbubble and ultrasound radiosensitization. Ultrasound Med Biol 2012;38:1212–1221.

Li C, Duric N, Littrup P, Huang L. *In vivo* breast sound-speed imaging with ultrasound tomography. Ultrasound Med Biol 2009;35:1615–1628.

Lizzi FL, Astor M, Liu T, Deng C, Coleman DJ, Silverman RH. Ultrasonic spectrum analysis for tissue assays and therapy evaluation. Int J Imaging Syst Technol 1997;8:3–10.

Lizzi FL, Greenebaum M, Feleppa EJ, Elbaum M, Coleman DJ. Theoretical framework for spectrum analysis in ultrasonic tissue characterization. J Acoust Soc Am 1983;73:1366–1373.

Luchies AC, Ghoshal G, O'Brien WD, Oelze ML. Quantitative ultrasonic characterization of diffuse scatterers in the presence of structures that produce coherent echoes. IEEE Trans Ultrason Ferroelectr Freq Control 2012;59:893–904.

Madsen EL, Zagzebski JA, Frank GR. Oil-in-gelatin dispersions for use as ultrasonically tissue-mimicking materials. Ultrasound Med Biol 1982;8:277–287.

McNemar Q. Note on the sampling error of the difference between correlated proportions or percentages. Psychometrika 1947;12:153–157.

Nam K, Rosado-Mendez IM, Wirtzfeld LA, Ghoshal G, Pawlicki AD, Madsen EL, Lavarello RJ, Oelze ML, Zagzebski JA, O'Brien WD, Hall TJ. Comparison of ultrasound attenuation and backscatter estimates in layered tissue-mimicking phantoms among three clinical scanners. Ultrason Imaging 2012;34:209–221.

Nam K, Rosado-Mendez IM, Wirtzfeld LA, Kumar V, Madsen EL, Ghoshal G, Pawlicki AD, Oelze ML, Lavarello RJ, Bigelow TA, Zagzebski JA, O'Brien WD, Hall TJ. Cross-imaging system comparison of backscatter coefficient estimates from a tissue-mimicking material. J Acoust Soc Am 2012;132:1319–1324.

Nam K, Rosado-Mendez IM, Wirtzfeld LA, Pawlicki AD, Kumar V, Madsen EL, Ghoshal G, Lavarello RJ, Oelze ML, Bigelow TA, Zagzebski JA, O'Brien WD, Hall TJ. Ultrasonic attenuation and backscatter coefficient estimates of rodent-tumor-mimicking structures: Comparison of results among clinical scanners. Ultrason Imaging 2011;33:233–250.

National Comprehensive Cancer Network. Invasive breast cancer version 1.2016, NCCN clinical practice guidelines in oncology. Natl Compr Cancer Netw 2016;14:324–354.

Oelze ML, O'Brien WD. Method of improved scatterer size estimation and application to parametric imaging using ultrasound. J Acoust Soc Am 2002;112:3053–3063.

Oelze ML, Zachary JF. Examination of cancer in mouse models using high-frequency quantitative ultrasound. Ultrasound Med Biol 2006;32:1639–1648.

Ogston KN, Miller ID, Payne S, Hutcheon AW, Sarkar TK, Smith I, Schofield A, Heys SD. A new histological grading system to assess response of breast cancers to primary chemotherapy: Prognostic significance and survival. Breast 2003;12:320–327.

Raum K, O'Brienjr WD. Pulse-echo field distribution measurement technique for high-frequency ultrasound sources. IEEE Trans Ultrason Ferroelectr Freq Control 1997;44:810–815.

Rosado-Mendez IM, Drehfal LC, Zagzebski JA, Hall TJ. Analysis of coherent and diffuse scattering using a reference phantom. IEEE Trans Ultrason Ferroelectr Freq Control 2016;63:1306–1320.

Rubovszky G, Horváth Z. Recent advances in the neoadjuvant treatment of breast cancer. J Breast Cancer 2017;20:119–131.

Sadeghi-Naini A, Falou O, Tadayyon H, Al-Mahrouki A, Tran W, Papanicolau N, Kolios MC, Czarnota GJ. Conventional frequency ultrasonic biomarkers of cancer treatment response *in vivo*. Transl Oncol 2013;6:234–243.

Sadeghi-Naini A, Papanicolau N, Falou O, Tadayyon H, Lee J, Zubovits J, Sadeghian A, Karshafian R, Al-Mahrouki A, Giles A, Kolios MC, Czarnota GJ. Low-frequency quantitative ultrasound imaging of cell death *in vivo*. Med Phys 2013;40:82901.

Sadeghi-Naini A, Papanicolau N, Falou O, Zubovits J, Dent R, Verma S, Tudeau ME, Boileau JF, Spayne J, Iradji S, Sofroni E, Lee J,

Lemon-Wong S, Yaffe MJ, Kolios MC, Czarnota GJ. Quantitative ultrasound evaluation of tumour cell death response in locally advanced breast cancer patients receiving chemotherapy. Clin Cancer Res 2013;19:2163–2174.

Sadeghi-Naini A, Sannachi L, Pritchard K, Trudeau M, Gandhi S, Wright FC, Zubovits J, Yaffe MJ, Kolios MC, Czarnota GJ. Early prediction of therapy responses and outcomes in breast cancer patients using quantitative ultrasound spectral texture. Oncotarget 2014;5:3497–3511.

Sadeghi-Naini A, Sannachi L, Tadayyon H, Tran WT, Slodkowska E, Trudeau M, Gandhi S, Pritchard K, Kolios MC, Czarnota GJ. Chemotherapy-response monitoring of breast cancer patients using quantitative ultrasound-based intra-tumour heterogeneities. Sci Rep 2017;7:10352.

Sannachi L, Tadayyon H, Sadeghi-Naini A, Tran W, Gandhi S, Wright F, Oelze M, Czarnota G. Non-invasive evaluation of breast cancer response to chemotherapy using quantitative ultrasonic backscatter parameters. Med Image Anal 2015;20:224–236.

Senkus E, Kyriakides S, Ohno S, Penault-Llorca F, Poortmans P, Rutgers E, Zackrisson S, Cardoso F, ESMO Guidelines Committee. Primary breast cancer: ESMO Clinical Practice Guidelines for diagnosis, treatment and follow-up. Ann Oncol 2015;26(Suppl 5):v8–v30.

Shen Q, Faraway J. An F test for linear models with functional responses. Statistica Sinica 2004;14:1239–1257.

Sun Y, Liao M, He L, Zhu C. Comparison of breast-conserving surgery with mastectomy in locally advanced breast cancer after good response to neoadjuvant chemotherapy: A PRISMA-compliant systematic review and meta-analysis. Medicine (Baltimore) 2017;96:e8367.

Tadayyon H, Sadeghi-Naini A, Czarnota GJ. Noninvasive characterization of locally advanced breast cancer using textural analysis of quantitative ultrasound parametric images. Transl Oncol 2014;7:759–767.

Vlad RM, Alajez NM, Giles A, Kolios MC, Czarnota GJ. Quantitative ultrasound characterization of cancer radiotherapy effects *in vitro*. Int J Radiat Oncol Biol Phys 2008;72:1236–1243.

Vlad RM, Brand S, Giles A, Kolios MC, Czarnota GJ. Quantitative ultrasound characterization of responses to radiotherapy in cancer mouse models. Clin Cancer Res 2009;15:2067–2075.

Wear KA, Wagner RF, Insana MF, Hall TJ. Application of autoregressive spectral analysis to cepstral estimation of mean scatterer spacing. IEEE Trans Ultrason Ferroelectr Freq Control 1993;40:50–58.

Wirtzfeld LA, Ghoshal G, Hafez ZT, Nam K, Labyed Y, Anderson JJ, Herd M-T, Haak A, He Z, Miller RJ, Sarwate S, Simpson DG, Zagzebski JA, Bigelow TA, Oelze ML, Hall TJ, O'Brien WD. Cross-imaging platform comparison of ultrasonic backscatter coefficient measurements of live rat tumors. J Ultrasound Med 2010;29:1117–1123.

Yang M, Krueger TM, Miller JG, Holland MR. Characterization of anisotropic myocardial backscatter using spectral slope, intercept and midband fit parameters. Ultrason Imaging 2007;29:122–134.

Yao LX, Zagzebski JA, Madsen EL. Backscatter coefficient measurements using a reference phantom to extract depth-dependent instrumentation factors. Ultrason Imaging 1990;12:58–70.